◆ Human Brain Mapping 29:1255–1264 (2008) ◆

Cortical Glucose Metabolism Correlates Negatively With Delta-Slowing and Spike-Frequency in Epilepsy Associated with Tuberous Sclerosis

Masaaki Nishida,[1] Eishi Asano,[1,2*] Csaba Juhász,[1,2] Otto Muzik,[1,3] Sandeep Sood,[4] and Harry T. Chugani[1,2,3]

[1]*Department of Pediatrics, Children's Hospital of Michigan, Wayne State University, Detroit, Michigan*
[2]*Department of Neurology, Children's Hospital of Michigan, Wayne State University, Detroit, Michigan*
[3]*Department of Radiology, Children's Hospital of Michigan, Wayne State University, Detroit, Michigan*
[4]*Department of Neurosurgery, Children's Hospital of Michigan, Wayne State University, Detroit, Michigan*

Abstract: The mechanism of altered glucose metabolism seen on positron emission tomography (PET) in focal epilepsy is not fully understood. We determined the association between interictal glucose metabolism and interictal neuronal activity, using PET and electrocorticography (ECoG) measures derived from 865 intracranial electrode sites in 11 children with focal epilepsy associated with tuberous sclerosis complex (TSC) (age: 0.5–16 years) undergoing epilepsy surgery. A multiple linear regression analysis was applied to each patient, to determine whether the glucose uptake at each electrode site on interictal PET was predicted by ECoG amplitude powers and interictal spike-frequency measured in the given electrode site. The regression slopes as well as *R*-square values (an indicator of fitness of the regression models) were finally averaged across the 11 patients. The mean regression slope for delta amplitude power was −0.0025 (95% CI: −0.0045 to −0.0004; $P = 0.02$ based on one-sample *t*-test) and that for spike frequency was −0.023 (95% CI: −0.042 to −0.0038; $P = 0.02$). On the other hand, the mean regression slopes for the remaining ECoG amplitude powers (theta, alpha, sigma, beta, and gamma activities) were not significantly different from zero. The mean *R*-square value was 0.39. These results suggest that increased delta-slowing and frequent spike activity were independently and additively associated with glucose hypometabolism in children with focal epilepsy associated with TSC. Association between frequent interictal spike activity and low glucose metabolism may be attributed to slow-wave components following spike discharges on ECoG recording, and a substantial proportion of the variance in regional glucose metabolism on PET could be explained by electrophysiological traits derived from conventional subdural ECoG recording. *Hum Brain Mapp 29:1255–1264, 2008.*

Key words: subdural electroencephalography recording; interictal spike-and-slow-wave; epilepsy surgery; cortical tubers; intracranial EEG

Additional Supporting Information may be found in the online version of this article.

Contract grant sponsor: NIH; Contract grant number: NS47550

*Correspondence to: Eishi Asano, Division of Pediatric Neurology, Children's Hospital of Michigan, Wayne State University, 3901 Beaubien St., Detroit, MI 48201, USA. E-mail: eishi@pet.wayne.edu

Received for publication 24 April 2007; Revised 27 June 2007; Accepted 9 July 2007

DOI: 10.1002/hbm.20461

Published online 19 October 2007 in Wiley InterScience (www.interscience.wiley.com).

INTRODUCTION

Positron emission tomography (PET) is a noninvasive functional imaging modality, which measures regional uptake of radiotracers designed to evaluate metabolism, blood flow, receptor binding properties, and other physiological processes in the human body, and PET imaging using 2-deoxy-2-[18F] fluoro-D-glucose (FDG) has been used to evaluate glucose metabolism patterns of human cerebral cortex [Chugani and Phelps, 1986; Phelps and Mazziotta, 1985]. Previous PET studies of patients with focal epilepsy associated with dysplastic lesions have shown that glucose is quite unevenly utilized in the cerebral cortex; the majority of dysplastic lesions, such as focal cortical dysplasia and cortical tubers, are hypometabolic on interictal FDG PET [Chugani et al., 1990; Kim et al., 2000; Rintahaka and Chugani, 1997; Szelies et al., 1983] and, in some cases, removal of the hypometabolic cortex associated with EEG abnormalities have resulted in good surgical outcomes [Chugani et al., 1990; Kim et al., 2000]. On the other hand, it has also been reported that the presumed epileptogenic focus can be hypermetabolic [Chugani et al., 1993; Engel et al., 1982] or normo-metabolic [Juhász et al., 2000] on interictal FDG PET in a substantial proportion of patients with focal epilepsy. Currently, no quantitative relationship has been demonstrated between the degree of glucose metabolism and the frequency of interictal spikes on scalp EEG [Engel et al., 1982; Lucignani et al., 1996], but a negative correlation between glucose metabolism in the lateral temporal cortex and its regional delta slowing on scalp EEG has been reported in adults with temporal lobe epilepsy [Erbayat Altay et al., 2005; Koutroumanidis et al., 1998].

Do electrophysiological traits other than delta slowing explain the variance of cortical glucose metabolism in individuals with focal epilepsy? We hypothesized that the fast-wave electrocorticography (ECoG) components derived from physiological and pathological neuronal activities were associated with high glucose metabolism, whereas slow-wave components were associated with decreased glucose metabolism in patients with focal epilepsy. In the present study of 11 children with focal epilepsy associated with tuberous sclerosis complex (TSC), we determined whether interictal subdural ECoG measures fitted into multiple regression equations could explain the variance of regional glucose metabolism on interictal FDG PET. We chose TSC as a model to study the relationship between glucose hypometabolism and ECoG traits, since TSC is an autosomal-dominant disorder characterized by cortical tubers, which are known to be stable in size over time, not preferentially localized to a certain location, and appear hypometabolic on FDG PET [Huttenlocher and Heydemann, 1984; Machado-Salas, 1984; Roach et al., 1998; Szelies et al., 1983].

METHODS

Patients

The inclusion criteria of the present study included: (i) age ranging from 5 months to 17 years, (ii) a diagnosis of uncontrolled focal seizures associated with TSC [Roach et al., 1998], (iii) a two-stage epilepsy surgery using extraoperative ECoG monitoring in Children's Hospital of Michigan, Detroit between May 2002 and October 2005, and (iv) 2-deoxy-2-[^{18}F] FDG PET performed within 12 months prior to the implantation of subdural electrodes. The exclusion criteria included history of previous epilepsy surgery. We studied a consecutive series of 11 children (age: 5 months–16 years; 5 girls and 6 boys) who met the inclusion criteria and satisfied the exclusion criteria (Table I). All 11 children underwent scalp video-EEG monitoring, MRI, FDG PET, and chronic intracranial ECoG monitoring with subdural electrodes as part of their pre-surgical evaluation. The study has been approved by the Institutional Review Board at Wayne State University, and written informed consent was obtained from the parents or guardians of all subjects.

MRI Procedure

MRI studies were performed on a GE Signa 1.5-Tesla scanner (GE Medical Systems, Milwaukee, WI) before sub-

TABLE I. Patient data

Patient number	Age at surgery	Gender	State during FDG PET uptake period	Location of interictal spikes on scalp EEG during FDG PET	Interval between PET and ECoG measurements (months)
1	0 year 5 months	M	Awake	Rt-C-P-T, Lt-C-P-T	2
2	1 year 2 months	M	Awake	Lt-C-F-T, Rt-P, Lt-P	4
3	1 year 6 months	M	Awake and sleep	Lt-C-P-T, Lt-F-T	3
4	1 year 11 months	F	Sleep	Rt-F-C, Rt-T, Rt-P, Lt-F-C	6
5	3 years 1 month	F	Awake	None	2
6	3 years 3 months	F	Awake	Lt-O, Lt-F, Lt-P-T, Lt-F-C-T, Rt-P-T	3
7	5 years 3 months	M	Sleep	Lt-T	9
8	6 years 7 months	M	Awake	Rt-T-O, Rt-O	6
9	7 years 5 months	F	Awake	Lt-P	9
10	9 years 9 months	F	Awake	Lt-O	12
11	16 years 0 month	M	Awake	None	3

y, year; mo, month; F, female; M, male; F, frontal; C, central; P, parietal; O, occipital; T, temporal.

dural electrode placement, as previously described [Juhász et al., 2000]. Anatomical/volumetric imaging of the whole brain was performed in all patients utilizing a T_1-weighted spoiled gradient echo (SPGR) sequence. The 3D SPGR sequence [repetition time (TR) 35 ms; echo time (TE) 5 ms; flip angle, 35°; slice thickness, 1.5 mm; field of view 240 mm] was acquired in the coronal plane.

PET Procedure

FDG PET studies were performed using the CTI/Siemens Exact/HR whole-body positron tomograph before Subdural electrode placement, as previously described [Juhász et al., 2000; Muzik et al., 1998]. In short, this scanner generates 47 image planes with a slice thickness of 3.125 mm, and the reconstructed image in-plane resolution obtained was 5.5 ± 0.35 mm full widths at half-maximum. Following a 40-min uptake period after the injection of FDG, a 20-min static scan was acquired. The scalp EEG was monitored throughout the uptake period to verify that all scans were interictal. Subsequently, we determined the state change (awake or sleep) of the patient during the first 20 min after FDG administration (Table I). None of the patients had seizures within 2 h before PET tracer injection or a secondarily generalized tonic clonic seizure within 8 h before PET tracer injection. The mean interval between PET scanning and subdural electrode placement was 5.4 months (range: 2–12 months).

Subdural Electrode Placement

For chronic intracranial ECoG recording, platinum grid electrodes (10 mm intercontact distance, 4 mm diameter; Ad-tech, Racine, WI) were surgically implanted as previously described [Asano et al., 2005]. Depth electrodes were also implanted as needed. The placement of intracranial electrodes was guided by the results of scalp video-EEG recording, MRI, interictal glucose metabolism on FDG PET, and interictal alpha-[^{11}C] methyl-L-tryptophan PET [Kagawa et al., 2005]. All electrode plates were stitched to adjacent plates and/or the edge of dura mater, to avoid movement of subdural electrodes after placement. In addition, intraoperative pictures were taken with a digital camera before dural closure to confirm the spatial accuracy of electrode display on three-dimensional brain surface reconstructed from MRI [Asano et al., 2005].

Extraoperative Video-ECoG Recording

Extraoperative video-ECoG recordings were performed as previously described [Asano et al., 2003, 2007]. Anti-epileptic medications were discontinued or reduced during ECoG monitoring until a sufficient number of habitual seizures (typically three seizures) were captured. A ground lead and a reference electrode were placed to the contralateral mastoid by a registered EEG technician. Surface EMG recordings from the left and right deltoid muscles were added as needed. ECoG data were obtained using a Stellate HARMONIE digital system [sampling rate: 200 Hz; Stellate, Quebec, Canada] for 3–5 days. Clinical manifestations were assessed using synchronized digital videos with 30 frames per second. Interictal epileptiform discharges [Asano et al., 2003], ictal discharges [Lee et al., 2000] and state changes [Asano et al., 2007] were visually assessed with a low-frequency filter of 0.5–1 Hz and high-frequency filter of 35–100 Hz. A low frequency filter of 3.0 Hz or higher was occasionally used to assess a low-amplitude fast wave activity.

Coregistration of PET, MRI, and Subdural Electrodes

Before subdural electrode placement, FDG PET, and MRI SPGR image volumes were coregistered as described previously [Juhász et al., 2000; Muzik, 1998; Pietrzyk et al., 1994], using MPI-Tool (Max-Planck-Institute, Cologne, Germany), which is a software package employing a multipurpose 3D registration technique. Following subdural electrode placement, planar X-ray images (lateral and anterior–posterior images) were acquired for determining the location of the electrodes on the brain surface. Three metallic fiducial markers were placed at anatomically well-defined locations on the patient's head for coregistration of the X-ray with the MRI as previously described [Juhász et al., 2000; von Stockhausen et al., 1997].

To reconstruct surface views corresponding to the planar X-ray image, three virtual markers were defined in the SPGR MR image volume at the same position as in the planar X-ray image, as previously described [Juhász et al., 2000; Muzik et al., 1998; von Stockhausen et al., 1997]. Using the software package "3D Tool" (Max-Planck-Institute, Cologne, Germany), a surface view was created, which corresponds to the planar X-ray image position, and where the location of electrodes was directly defined on the brain surface. The accuracy of this procedure was reported previously as 1.24 ± 0.66 mm with a maximal misregistration of 2.7 mm [von Stockhausen et al., 1997) and was confirmed by intraoperative digital photographs showing in situ locations of the subdural electrodes [Asano et al., 2005]. Anatomical landmarks (central sulcus, Sylvian fissure, and gyral pattern) that were readily identifiable on both the photographs and the 3D-reconstructed brain surface were used to verify the exact location of the electrodes. Following coregistration of the subdural grid with the surface view, virtual spheres were created at those locations on the brain surface to represent a projection of the electrodes onto the surface. These spheres mark the position of the electrodes on the cortical surface and allow the assessment of intracranial electrode location relative to the MRI and FDG PET metabolism from varying view angles.

Ranking Cortical Glucose Metabolism on Each Subdural Electrode Site

Glucose metabolism values were rescaled into six fractional units (ranks) with equal range as follows: 0.0

(lowest), 0.2, 0.4, 0.6, 0.8, and 1.0 (highest), using the software package "3D Tool." Subsequently, rescaled PET metabolism was delineated with different colors on each individual 3D-brain surface image (supplementary Fig. S1). Each subdural electrode site was assigned a PET fractional rank shown earlier, according to the color scale within the brain immediately below each electrode seen on the 3D-brain surface image. A subdural electrode located on a boundary between distinct PET colors was given a PET fractional rank, based on the larger size of PET color under the electrode. This method allows more rapid estimation of cortical glucose metabolism, compared with an alternative method of computation of glucose metabolism by drawing regions of interest in each cortical area as performed in previous studies [Asano et al., 2000; Kagawa et al., 2005].

Quantitative Measurement of Interictal ECoG Amplitude Powers

ECoG amplitude powers for each subdural electrode site were quantitatively measured using a method similar to that reported in previous ECoG studies [Asano et al., 2004, 2005; Gotman et al., 1993]. subdural electrodes showing artifacts [Klem, 2003], depth electrodes, epidural electrodes, electrodes overlying another electrode array, and electrodes facing the presumed nonepileptic hemisphere via the falx were excluded from further analysis, and a total of 865 subdural electrodes (48–99 electrodes per subject) were analyzed. The quantitative ECoG analysis was performed using the Stellate SENSA software [Asano et al., 2003, 2007; Gotman et al., 1993].

First, ECoG signals were remontaged to an average reference, to obtain reference-free topographic maps of spectral measures [Crone et al., 1998]. A 10-min ECoG segment during quiet wakefulness and another segment during sleep were selected from the interictal extraoperative ECoG data, based on the following criteria: at least 8 h after a secondarily generalized tonic clonic seizure and at least 2 h after other types of clinical seizures [Asano et al., 2005, 2007]. A consecutive series of 5.12-s epochs were placed over the 10-min awake ECoG segment as well as the 10-min sleep segment. After the placement of consecutive epochs, an amplitude spectrum (x-axis unit: Hz; y-axis unit: μV/Hz) was created for each epoch and each channel, using a Fast Fourier Transformation. The software Subsequently displayed the ECoG amplitude power (unit: μV) at each epoch within preset frequency bands, which was calculated as the summation of all frequency components under the amplitude spectral curve within the given frequency band. The frequency bands were preset as follows: 0.5–4.0 Hz (delta band), 4.0–8.0 Hz (theta band), 8.0–12.0 Hz (alpha band), 12–16 Hz (sigma band), 16–32 Hz (beta band), 32–64 Hz (low-frequency gamma band), and 64–100 Hz (high-frequency gamma band) [Asano et al., 2005]. The ECoG amplitude power of 32–64 Hz was calculated without a 56–64 Hz component, if visual inspection revealed a 60 Hz artifact peak on the amplitude spectral curve for all subdural electrodes [Asano et al., 2004]. Subsequently, ECoG amplitude powers for the earlier-mentioned frequency bands were averaged across the whole awake epochs and separately averaged across the whole sleep epochs. This procedure finally yielded the mean ECoG amplitude powers for (i) "delta," (ii) "theta," (iii) "alpha," (iv) "sigma," (v) "beta," (vi) "low-frequency gamma," and (vii) "high-frequency gamma" bands, for each electrode site, and for each state (Fig. 1 and supplementary Figs. S2 and S3).

Quantitative Analysis of Spike Frequency Recorded on ECoG

Quantitative analysis of interictal spike frequency was performed on the ECoG, using Stellate SENSA software [Asano et al., 2003, 2007; Gotman and Gloor, 1976]. The same 10-min awake and sleep segments used in the power amplitude analysis were utilized for spike frequency analysis. It has been reported that the spatial distribution of interictal spike frequency is similar between 10-min awake and sleep ECoG segments in children with focal epilepsy [Asano et al., 2007]. Each electrode site was given a spike frequency measure during wakefulness as well as that during sleep (Fig. 1 and supplementary Figs. S2 and S3).

Delineation of ECoG Data on 3D-Reconstructed MRI

Quantitative measures including ECoG amplitude powers as well as interictal spike frequency were delineated on each individual 3D-reconstructed MRI (Fig. 1 and supplementary Figs. S2 and S3) as previously described [Asano et al., 2005]. Electrode positions (x- and y-axis values) on the planar X-ray coordinate were measured for every electrode using Microsoft PowerPoint (Microsoft, Redmond, WA), and were registered into the SurGe Interpolation Software (Web site: http://mujweb.cz/www/SurGe/surgemain.htm). The topographic map derived from the skull X-ray images was used to display the earlier-mentioned ECoG measures on the 3D-reconstructed surface image.

Statistical Analysis

A multiple linear regression model was applied to each individual patient to predict the PET fractional rank (a measure of glucose uptake) in each electrode site using ECoG measures in the given electrode site. Thereby, the outcome measure was the PET fractional rank and treated as a continuous variable. ECoG measures as predictors included (i) "delta amplitude power," (ii) "theta amplitude power," (iii) "alpha amplitude power," (iv) "sigma amplitude power," (v) "beta amplitude power," (vi) "low-frequency gamma amplitude power," (vii) "high-frequency

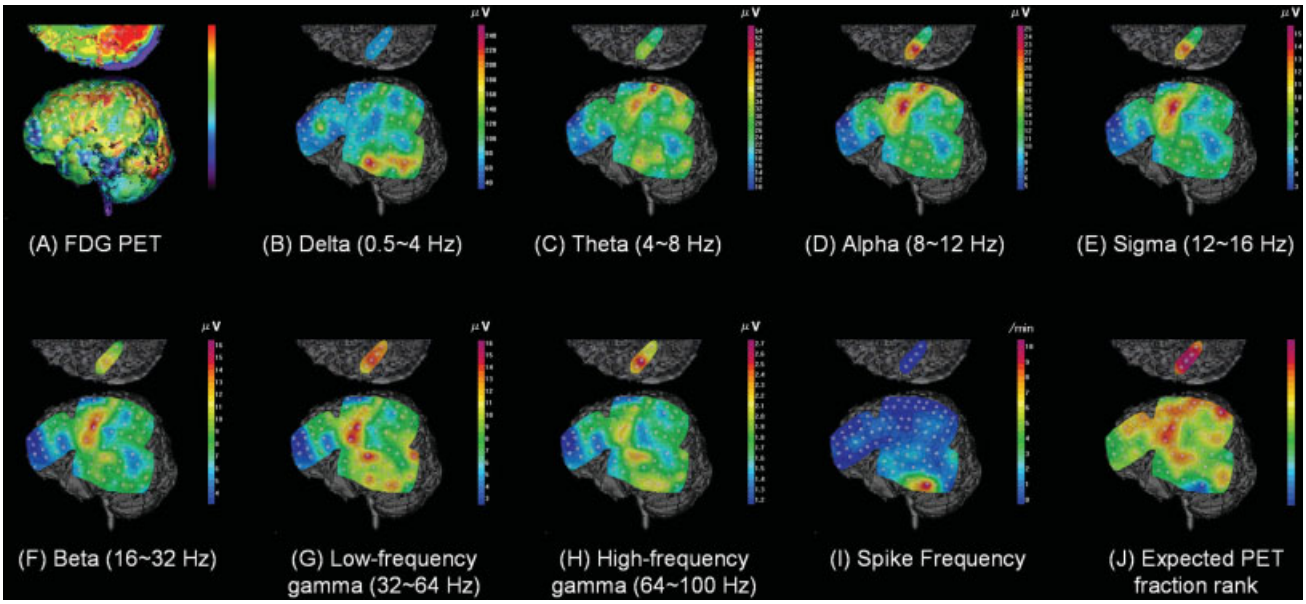

Figure 1.

FDG PET and ECoG measures in a 14-month-old boy with uncontrolled seizures associated with tuberous sclerosis complex. (**A**) Interictal FDG PET showed nodular glucose hypometabolic regions involving the left temporal, frontal and parietal regions. (**B**–**I**) Topographic map of spectral amplitude power and interictal spike activity. The largest hypometabolic area in the left temporal region was associated with increased delta amplitude power as well as increased spike frequency. (**J**) Topography of PET fractional ranks expected from the regression model: $Y_{PET} = 0.21 + 0.0012 \times X_D - 0.018 \times X_T + 0.079 \times X_A - 0.18 \times X_S + 0.14 \times X_B - 0.14 \times X_{LG} + 0.47 \times X_{HG} - 0.091 \times X_{SP}$ The *R*-square value for this regression model was 0.53.

gamma amplitude power," and (viii) "interictal spike frequency."

ECoG measures during wakefulness were utilized in 8 patients (Nos. 1, 2, 6, 7, 9, 10, 11, and 12) who were awake during the first 20-min PET uptake period, whereas ECoG measures during sleep were utilized in 2 patients (Nos. 5 and 8) who were asleep during PET uptake period. In patient No. 3, who was awake for the first 8 min and asleep for the subsequent 12 min during the PET uptake period, weighted-average ECoG measures (40% from awake segments and 60% from sleep) were utilized. This approach was taken, since a previous study showed that glucose PET pattern during awake state differed from that during sleep in normal controls [Buchsbaum et al., 2001].

A multiple regression model tested in the present study is shown below.

$$Y_{PETi} = \beta_{0i} + \beta_{Di} \times X_{Di} + \beta_{Ti} \times X_{Ti} + \beta_{Ai} \times X_{Ai} + \beta_{Si} \times X_{Si} + \beta_{Bi} \times X_{Bi} + \beta_{LGi} \times X_{LGi} + \beta_{HGi} \times X_{HGi} + \beta_{SPi} \times X_{SPi},$$

where (Y_{PETi}) represented the expected PET fractional rank in a subdural electrode site showing a delta amplitude power of (X_{Di}), a theta amplitude power of (X_{Ti}), an alpha amplitude power of (X_{Ai}), a sigma power of (X_{Si}), a beta amplitude power of (X_{Bi}), a low-frequency gamma amplitude power of (X_{LGi}), a high-frequency gamma amplitude power of (X_{HGi}), and interictal spike frequency of (X_{SPi}) in subject i (i = 1, 2,. . ., and 11). Thereby, subject i was assigned a regression slope for "delta amplitude power" (β_{Di}), "that for theta amplitude power" (β_{Ti}), "that for alpha amplitude power" (β_{Ai}), "that for sigma amplitude power" (β_{Si}), "that for beta amplitude power" (β_{Bi}), "that for low-frequency gamma amplitude power" (β_{LGi}), "that for high-frequency gamma amplitude power" (β_{HGi}), and "that for interictal spike frequency" (β_{SPi}). Each regression model assigned to each subject yielded an *R*-square value (an indicator of fitness of the regression models).

Subsequently, the one-sample *t*-test was applied to the means of each regression slope. The statistical null hypothesis was that each of the mean regression slopes averaged among 11 subjects (mean β_D, mean β_T, mean β_A, mean β_S, mean β_B, mean β_{LG}, mean β_{HG}, and mean β_{SP}) was zero, whereas the alternative hypothesis was that each mean regression slope was different from zero. A significance level of 0.05 was used, and a 95% confidence interval (95% CI) was calculated for the mean of each regression slope. Similarly, the mean *R*-square value across the 11 subjects was calculated.

Finally, association between "the model fitness represented by an *R*-square value" and "the PET-ECoG interval" was assessed using a linear regression analysis (supplementary Fig. S4), to determine whether a long interval between PET and ECoG studies was a factor decreasing

TABLE II. Mean regression slopes for ECoG measures and mean *R*-square value for the regression models

	Mean among the 11 subjects	95% Cl	P-Value
Intercept (β_o)	0.57	(0.41, 0.73)	<0.001
Regression slope for 'delta amplitude power' (β_D)	−0.0025	(−0.0045, −0.0004)	0.02
Regression slope for 'theta amplitude power' (β_T)	−0.0072	(−0.017, 0.0025)	0.1
Regression slope for 'alpha amplitude power' (β_A)	0.0051	(0.021, 0.031)	0.7
Regression slope for 'sigma amplitude power' (β_S)	0.054	(−0.018, 0.13)	0.1
Regression slope for 'beta amplitude power' (βB)	−0.014	(−0.079, 0.051)	0.6
Regression slope for 'gamma amplitude power' (β_{LG})	−0.021	(−0.081, 0.040)	0.5
Regression slope for 'gamma amplitude power' (β_{HG})	0.044	(−0.086, 0.17)	0.5
Regression slope for 'spike amplitude power' (β_{SP})	−0.023	(−0.042, −0.0038)	0.02
R−Square	0.39	NA	NA

The mean regression slope for delta amplitude power as well as that for interictal spike frequency was significantly smaller than zero. Each *P*- value was derived from a one sample *t*-test where the null hypothesis was that the mean regression slope was zero whereas the alternative hypothesis was that the regression slope was different from zero.

the association between PET and ECoG measures. All statistical analyses were performed using the computer software SAS® 9.1 (SAS Institute, Cary, NC).

RESULTS

Individual FDG PET and ECoG data in three cases are presented in Figure 1 and supplementary Figures S2 and S3. The range and mean of ECoG measures for all subjects are presented in supplementary Table SI. Visual assessment revealed that the areas showing glucose hypometabolism were larger than those of MRI-visible tubers in all patients, as previously reported [Asano et al., 2000]. Visual assessment also revealed that focal delta slowing predominantly involved the center of glucose-hypometabolic cortex overlying a cortical tuber, and the degree of delta slowing appeared less prominent in the periphery of glucose hypometabolic areas. The electrode showing the greatest spike frequency was located in the center of glucose hypometabolic area in six children (patients nos. 2, 4, 5, 8, 9, and 11) and located on the margin of glucose hypometablosm in the remaining five children.

The mean regression slopes as well as the mean *R*-square values averaged across the 11 subjects are presented in Table II. The mean regression slope for delta amplitude power (=mean β_D) was −0.0025 (95% CI: −0.0045 to −0.0004; $P = 0.02$ based on one sample *t*-test) and that for spike frequency (=mean β_{SP}) was −0.023 (95% CI: −0.042 to −0.0038; $P = 0.02$). These results indicated that each 1 μV increase in delta amplitude power was associated with a decrease in a PET fractional rank by 0.0025, and that each 1 per min increase in spike frequency was associated with a decrease in a PET fractional rank by 0.023. On the other hand, the mean regression slope for the remaining ECoG amplitude powers (theta, alpha, sigma, beta, or gamma activities) were not significantly different from zero (Table II).

The mean *R*-square value across the 11 subjects was 0.39 (range: 0.27–0.68); thus, about 40% of the variance of PET fractional ranks among electrodes were explained by the multiple linear regression models using the earlier-mentioned eight ECoG measures in the given electrode site.

The "interval between PET and ECoG studies in each subject" and "the *R*-square value derived from the regression model" are plotted in supplementary Figure S4. There was no statistically significant linear association between "the interval between PET and ECoG studies" and "the *R*-square value derived from the regression model" ($P = 0.2$ based on linear regression analysis).

DISCUSSION

The present study demonstrates that regional glucose uptake measured by interictal FDG PET was negatively correlated to delta activity (0.5–4.0 Hz) and interictal spike frequency recorded in intracranial electrode sites in children with focal epilepsy associated with TSC. On the other hand, the study failed to prove a quantitative linear association between regional glucose metabolism and the remaining ECoG measures (theta, alpha, sigma, beta, or gamma activities). Independent and additive association between "glucose hypometabolism on PET" and "delta slowing" and "interictal spike frequency on ECoG" is a novel finding in the present study, and the results increase our understanding of the pathophysiology of altered cortical metabolism in relation to electrophysiology in children with focal epilepsy associated with dysplastic lesions.

Significance of Delta Slowing in Relation to Cortical Glucose Metabolism

In the present study, a delta-range amplitude power value in each electrode site probably consisted of physiological and pathological components. It is well known that delta slowing is diffusely increased during non-REM sleep in healthy humans [Nekhorocheff, 1950] and increased proportion of delta wave activity is one of the criteria for definition of sleep stages [Erwin et al., 1984; Nekhorocheff,

1950]. Previous studies using [^{15}O]-water PET and scalp EEG showed that delta wave activity was increased during non-REM sleep and the magnitude of delta wave activity was negatively correlated to cerebral blood flow in healthy volunteers [Dang-Vu et al., 2005; Hofle et al., 1997].

A relationship between pathological delta slowing and regional glucose hypometabolism has been shown in previous studies. For example, studies in dogs and rodents using ECoG recording have demonstrated that delta wave amplitude is increased on a real-time basis when a regional cerebral lesion is artificially produced by arterial occlusion or a toxic substance [Carpentier et al., 2001; Gurvitch and Ginsburg, 1977; Hartings et al., 2006]. Studies of Alzheimer's disease [Valladares-Neto et al., 1995] and vascular dementia [Szelies et al., 1999] patients have found that the magnitude of delta slowing on scalp EEG was negatively correlated to cerebral glucose metabolism on PET. Studies of adults with temporal lobe epilepsy revealed that the magnitude of delta slowing in the lateral temporal cortex was negatively correlated to regional glucose metabolism in that area [Erbayat Altay et al., 2005; Koutroumanidis et al., 1998]. Taken together, delta wave activity recorded on interictal ECoG may be an indicator of underlying low neuronal activity.

Significance of Frequent Interictal Spikes in Relation to Cortical Glucose Metabolism

It is still uncertain whether interictal epileptiform discharges represent excitatory, inhibitory or a combination of the two. Studies in cats using intracellular electrophysiology recording [Contreras et al., 1997; Fisher and Prince, 1977] as well as a study of adults with temporal lobe epilepsy using paired pulse stimulation [Wilson et al., 1998] suggested that the slow-wave component of interictal spike-and-wave discharges represented inhibitory postsynaptic potentials, which temporarily inactivated cortical function. A study of adults with focal epilepsy using ECoG showed that maximum delta activity coincided spatially with or adjacent to the cortical area showing maximum spiking in 22 out of 40 cases [Panet-Raymond and Gotman, 1990]. Recent studies using simultaneous recording of functional MRI and scalp EEG showed that interictal epileptiform discharges were associated with regional deactivation in the presumed epileptogenic focus and the surrounding cortex in a subset of patients with focal epilepsy [Federico et al., 2005; Kobayashi et al., 2006], and it was reported that spike-and-slow waves were always associated with deactivation, which was not observed with spikes not followed by a slow wave [Kobayashi et al., 2006]. Another study using functional MRI showed that blood oxygenation level-dependent responses associated with interictal epileptiform discharges were predominantly positive in the thalamus and predominantly negative in the cortex in patients with idiopathic and secondarily generalized epilepsy [Hamandi et al., 2006]. Association between glucose hypometabolism and frequent interictal epileptiform discharges found in the present study might be attributed to slow-wave EEG components following spikes.

The association between frequent spiking and glucose hypometabolism shown in the present study seems to be inconsistent with the previous observations that many epileptic patients with very frequent interictal spiking activities [Chugani et al., 1993], continuous spike-and-wave during slow-wave sleep [Luat et al., 2005] or periodic lateralized epileptiform discharges [Handforth et al., 1994] had regional glucose hypermetabolism on FDG PET. Further studies on epileptic patients with focal hyper- and hypometabolism on PET may determine the electrophysiological traits distinctively associated with glucose hypermetabolism and hypometabolism in the future.

Causal Relationship Between Interictal Neuronal Activity and Cortical Glucose Metabolism

The present study was not designed to determine the causal relationship but association between regional interictal neuronal activity and cortical glucose metabolism in children with focal epilepsy with TSC. Thus, it is still unknown whether interictal neuronal activity "drives" or "is driven by" the metabolism of cortical tissue exerting this activity. Previous human studies using transcranial magnetic stimulation have shown that low frequency (1 Hz) stimulation decreases the amplitude of motor-evoked potentials, indicating decreased excitability [Chen et al., 1997], whereas stimulation at the rate of 5–10 Hz had the opposite effect [Berardelli et al., 1998; Pascual-Leone et al., 1994]. Furthermore, studies using rat hippocampal and amygdale slice preparation demonstrated that in vitro electrical stimulation using low-frequency rate induces long-term depression of neurons under some conditions, whereas acute high-frequency stimulation induced long-term potentiation [Li et al., 1998; Malenka, 1994]. Recent studies using functional MRI combined with simultaneous scalp EEG recording have suggested that interictal epileptiform activity was frequently associated with subsequent alteration of blood oxygenation level-dependent signals in adults with focal epilepsy [Gotman et al., 2006; Kobayashi et al., 2006]. These observations suggest that dynamic neuronal activity may, in part, determine FDG PET patterns in individuals with focal epilepsy.

On the other hand, morphological studies have suggested that cortical hypometabolism in TSC may be due to decreased numbers of neurons and abnormal dendritic pattern in the cortical tubers, and that such abnormal neurons with smaller membrane areas would require less energy to maintain cellular membrane potentials [Huttenlocher and Heydemann, 1984; Machado-Salas, 1984]. These observations suggest that interictal baseline neuronal activity determined by the morphology of structural lesions may also contribute to the hypometabolism seen on interictal FDG PET.

Methodological Considerations

The combined analysis of PET and quantitative intracranial ECoG measures on an individual electrode basis was a novel approach used in the present study. Yet, there were several methodological limitations. First, although both PET and ECoG studies for a given patient were obtained during the interictal state, these were not obtained simultaneously. Although a number of investigators have studied the relationship between PET and subdural ECoG measures in patients with epilepsy [Asano et al., 2005; Henry et al., 1993; Juhász et al., 2000; Luat et al., 2005; Olson et al., 1990], none of the previous studies obtained simultaneous PET-ECoG recordings. In the present study, we attempted to match the conditions between the two series, as previously performed in a study combining PET and 1H magnetic resonance spectroscopy [Pfund et al., 2000]. Patients who underwent PET more than 12 months before ECoG recording were excluded from the present study; none of the PET or ECoG data analyzed were derived from the postical state, and interictal ECoG segments were selected according to the state (awake or sleep) during the first 20 min of the FDG PET uptake period. Yet, conditions between the two recordings almost certainly were different in the present study. Non-simultaneous recordings may have led to the variance of PET imaging pattern, which could not be explained by the multiple linear regression model using the ECoG measures in the given electrode site. In the present study, we determined whether a longer interval between PET and ECoG studies was associated with a lower model fit in the regression equation in a given subject, and the results suggested no statistically significant association between the interval between PET and ECoG studies and the degree of model fit represented by an *R*-square value (supplementary Fig. S4).

The limitation of multiple regression analysis includes "collinearity among the predictor variables," which can potentially compromise the model [Cohen et al., 2002]. In other words, failure to prove a statistically-significant correlation between the PET fractional rank and ECoG amplitude powers other than delta amplitude power does not necessarily mean that ECoG components other than delta-wave did not explain the variance of regional glucose metabolism on PET at all. Since ECoG amplitude power at a frequency band was certainly correlated to ECoG amplitude powers at other frequency bands, it is possible that the predictive effect of an ECoG amplitude power on PET measures may have been eliminated by more dominant predictive effect of ECoG amplitude power at another frequency band.

Factors which may affect PET and ECoG findings include antiepileptic medications and intracranial electrode placement. Previous scalp EEG and intracranial ECoG studies in adults with focal epilepsy suggested that interictal spike frequency was increased during the post-ictal period but not simply after a decrease in medication [Gotman and Koffler, 1989; Gotman and Marciani, 1985]. It has been reported that cerebral metabolic rates for glucose are globally decreased by several antiepileptic drugs [Spanaki et al., 1999; Theodore, 1988]. However, use of multiple regression approach with glucose metabolism as an outcome variable rescaled into six fractional units eliminated such global effects of these medications on PET. Therefore, the effects of antiepileptic drugs on FDG PET studies are considered to be relatively small in the present study.

It has also been reported that placement of intracranial electrodes increases intracranial pressure (ICP) in patients with focal epilepsy [Shah et al., 2007]. A previous [^{15}O]-water PET study of children with hydrocephalus reported that increased ICP was associated with global decrease in cerebral blood flow [Klinge et al., 1998]. Again, use of a multiple regression approach eliminated such global effects of pressure on ECoG measures.

Previous studies of adults with temporal lobe epilepsy using PET and EEG applied an asymmetry index approach to determine PET abnormalities [Erbayat Altay et al., 2005; Koutroumanidis et al., 1998]. In other words, PET abnormalities in the lateral temporal cortex were determined by comparing its regional glucose metabolism to that in the contralateral homotopic area, which was assumed to have normal glucose metabolism. This asymmetry index approach was not used in the present study of TSC because an assumption of normal glucose metabolism in the contralateral hemisphere was not tenable.

Future Direction

In the present study, ECoG was recorded with a sampling frequency of 200 Hz as previously described [Asano et al., 2005]; we were not able to analyze ECoG activities above Nyquist frequency, which was 100 Hz in the present study. Thus, the logical next step in the research of interictal FDG PET and ECoG relationships would be to analyze ECoG data recorded with higher sampling frequency to determine how gamma activities above 100 Hz can explain the variance of metabolism pattern on FDG PET. Particularly, gamma activities in area close to glucose hypometabolism may facilitate our understanding of the mechanism of interictal and ictal discharges.

A longitudinal study on the same individuals with focal epilepsy as well as a study of patients with etiologies other than TSC (such as non-lesional focal epilepsy) may also increase our understanding of the relationship between interictal neuronal activity and glucose metabolism and potentially elucidate the pathophysiology of interictal hypermetabolism on FDG PET. Finally, we plan to apply quantitative interictal PET and ECoG analysis for pediatric epilepsy surgery subjects, to formulate a model for prediction of surgical outcome.

ACKNOWLEDGMENTS

We are grateful to Aashit Shah, M.D., Jagdish Shah, M.D., Carol Pawlak, R. EEG/EP. T., and Ruth Roeder,

R.N., M.S. and the staff of the Division of Electroneurodiagnostics at Children's Hospital of Michigan, Wayne State University for the collaboration and assistance in performing the studies described earlier. We also appreciate Brenda Gillespie, Ph.D. and Trivellore Eachambadi Raghunathan, Ph.D. in the School of Public Health at University of Michigan for their advice on the statistical analysis.

REFERENCES

Asano E, Chugani DC, Muzik O, Shen C, Juhász C, Janisse J, Ager J, Canady A, Shah JR, Shah AK, Watson C, Chugani HT (2000): Multimodality imaging for improved detection of epileptogenic foci in tuberous sclerosis complex. Neurology 54:1976–1984.

Asano E, Muzik O, Shah A, Juhász C, Chugani DC, Sood S, Janisse J, Ergun EL, Ahn-Ewing J, Shen C, Gotman J, Chugani HT (2003): Quantitative interictal subdural EEG analysis in children with neocortical epilepsy. Epilepsia 44:425–434.

Asano E, Muzik O, Shah A, Juhász C, Chugani DC, Kagawa K, Benedek K, Sood S, Gotman J, Chugani HT (2004): Quantitative visualization of ictal subdural EEG changes in children with neocortical focal seizures. Clin Neurophysiol 115:2718–2727.

Asano E, Juhász C, Shah A, Muzik O, Chugani DC, Shah J, Sood S, Chugani HT (2005): Origin and propagation of epileptic spasms delineated on electrocorticography. Epilepsia 46:1086–1097.

Asano E, Mihaylova T, Juhasz C, Sood S, Chugani HT (2007): Effect of sleep on interictal spikes and distribution of sleep spindles on electrocorticography in children with focal epilepsy. Clin Neurophysiol 118:1360–1368.

Berardelli A, Inghilleri M, Rothwell JC, Romeo S, Curra A, Gilio F, Modugno N, Manfredi M (1998): Facilitation of muscle evoked responses after repetitive cortical stimulation in man. Exp Brain Res 122:79–84.

Buchsbaum MS, Hazlett EA, Wu J, Bunney WE (2001): Positron emission tomography with deoxyglucose-F18 imaging of sleep. Neuropsychopharmacology 25 (Suppl 5):S50– S56.

Carpentier P, Foquin A, Dorandeu F, Lallement G (2001): Delta activity as an early indicator for soman-induced brain damage: A review. Neurotoxicology 22:299–315.

Chen R, Classen J, Gerloff C, Celnik P, Wassermann EM, Hallett M, Cohen LG (1997): Depression of motor cortex excitability by low-frequency transcranial magnetic stimulation. Neurology 48:1398–1403.

Chugani HT, Phelps ME (1986): Maturational changes in cerebral function in infants determined by 18FDG positron emission tomography. Science 231:840–843.

Chugani HT, Shields WD, Shewmon DA, Olson DM, Phelps ME, Peacock WJ (1990): Infantile spasms. I. PET identifies focal cortical dysgenesis in cryptogenic cases for surgical treatment. Ann Neurol 27:406–413.

Chugani HT, Shewmon DA, Khanna S, Phelps ME (1993): Interictal and postictal focal hypermetabolism on positron emission tomography. Pediatr Neurol 9:10–15.

Cohen J, Cohen P, West SG, Aiken LS (2002): Applied Multiple Regression—Correlation Analysis for the Behavioral Sciences, 3rd ed. Mahwah, NJ: Lawrence Erlbaum Associates.

Contreras D, Destexhe A, Steriade M (1997): Intracellular and computational characterization of the intracortical inhibitory control of synchronized thalamic inputs in vivo. J Neurophysiol 78:335–350.

Crone NE, Miglioretti DL, Gordon B, Lesser RP (1998): Functional mapping of human sensorimotor cortex with electrocorticographic spectral analysis. II. Event-related synchronization in the gamma band. Brain 121:2301–2315.

Dang-Vu TT, Desseilles M, Laureys S, Degueldre C, Perrin F, Phillips C, Maquet P, Peigneux P (2005): Cerebral correlates of delta waves during non-REM sleep revisited. Neuroimage 28:14–21.

Engel J Jr, Kuhl DE, Phelps ME, Mazziotta JC (1982): Interictal cerebral glucose metabolism in partial epilepsy and its relation to EEG changes. Ann Neurol 12:510–517.

Altay EE, Fessler AJ, Gallagher M, Attarian HP, Dehdashti F, Vahle VJ, Ojemann J, Dowling JL, Gilliam FG (2005): Correlation of severity of FDG-PET hypometabolism and interictal regional delta slowing in temporal lobe epilepsy. Epilepsia 46: 573–576.

Erwin CW, Somerville ER, Radtke RA (1984): A review of electroencephalographic features of normal sleep. J Clin Neurophysiol 1:253–274.

Federico P, Archer JS, Abbott DF, Jackson GD (2005): Cortical/subcortical BOLD changes associated with epileptic discharges: An EEG-fMRI study at 3 T. Neurology 64:1125–1130.

Fisher RS, Prince DA (1977): Spike-wave rhythms in cat cortex induced by parenteral penicillin. II. Cellular features. Electroencephalogr Clin Neurophysiol 42:625–639.

Gotman J, Gloor P (1976): Automatic recognition and quantification of interictal epileptic activity in the human scalp EEG. Electroencephalogr Clin Neurophysiol 41:513–529.

Gotman J, Koffler DJ (1989): Interictal spiking increases after seizures but does not after decrease in medication. Electroencephalogr Clin Neurophysiol 72:7–15.

Gotman J, Marciani MG (1985): Electroencephalographic spiking activity, drug levels, and seizure occurrence in epileptic patients. Ann Neurol 17:597–603.

Gotman J, Levtova V, Farine B (1993): Graphic representation of the EEG during epileptic seizures. Electroencephalogr Clin Neurophysiol 87:206–214.

Gotman J, Kobayashi E, Bagshaw AP, Benar CG, Dubeau F (2006): Combining EEG and fMRI: A multimodal tool for epilepsy research. J Magn Reson Imaging 23:906–920.

Gurvitch AM, Ginsburg DA (1977): Types of hypoxic and posthypoxic delta activity in animals and man. Electroencephalogr Clin Neurophysiol 42:297–308.

Hamandi K, Salek-Haddadi A, Laufs H, Liston A, Friston K, Fish DR, Duncan JS, Lemieux L (2006): EEG-fMRI of idiopathic and secondarily generalized epilepsies. Neuroimage 31:1700–1710.

Handforth A, Cheng JT, Mandelkern MA, Treiman DM (1994): Markedly increased mesiotemporal lobe metabolism in a case with PLEDs: Further evidence that PLEDs are a manifestation of partial status epilepticus. Epilepsia 35:876–881.

Hartings JA, Tortella FC, Rolli ML (2006): AC electrocorticographic correlates of peri-infarct depolarizations during transient focal ischemia and reperfusion. J Cereb Blood Flow Metab 26:696–707.

Henry TR, Mazziotta JC, Engel J Jr (1993): Interictal metabolic anatomy of mesial temporal lobe epilepsy. Arch Neurol 50: 582–589.

Hofle N, Paus T, Reutens D, Fiset P, Gotman J, Evans AC, Jones BE (1997): Regional cerebral blood flow changes as a function of delta and spindle activity during slow wave sleep in humans. J Neurosci 17:4800–4808.

Huttenlocher PR, Heydemann PT (1984): Fine structure of cortical tubers in tuberous sclerosis: A Golgi study. Ann Neurol 16:595–602.

Juhász C, Chugani DC, Muzik O, Watson C, Shah J, Shah A, Chugani HT (2000): Is epileptogenic cortex truly hypometabolic on ictal positron emission tomography? Ann Neurol 48:88–96.

Kagawa K, Chugani DC, Asano E, Juhász C, Muzik O, Shah A, Shah J, Sood S, Kupsky WJ, Mangner TJ, Chakraborty PK, Chugani HT (2005): Epilepsy surgery outcome in children with tuberous sclerosis complex evaluated with alpha-[11C]methyl-L-tryptophan positron emission tomography (PET). J Child Neurol 20:429–438.

Kim SK, Na DG, Byun HS, Kim SE, Suh YL, Choi JY, Yoon HK, Han BK (2000): Focal cortical dysplasia: Comparison of MRI and FDG-PET. J Comput Assist Tomogr 24:296–302.

Klem GH (2003): Artifacts. In: Ebersole JS, Pedley TA, editors. Current Practice of Clinical Electroencephalography. New York: Lippincott Williams and Wilkins. pp 271–287.

Klinge P, Fischer J, Brinker T, Heissler HE, Burchert W, Berding G, Knapp WH, Samii M (1998): PET and CBF studies of chronic hydrocephalus: A contribution to surgical indication and prognosis. J Neuroimaging 8:205–209.

Kobayashi E, Bagshaw AP, Grova C, Dubeau F, Gotman J (2006): Negative BOLD responses to epileptic spikes. Hum Brain Mapp 27:488–497.

Koutroumanidis M, Binnie CD, Elwes RD, Polkey CE, Seed P, Alarcon G, Cox T, Barrington S, Marsden P, Maisey MN, Panayiotopoulos CP (1998): Interictal regional slow activity in temporal lobe epilepsy correlates with lateral temporal hypometabolism as imaged with 18FDG PET: Neurophysiological and metabolic implications. J Neurol Neurosurg Psychiatry 65:170–176.

Lee SA, Spencer DD, Spencer SS (2000): Intracranial EEG seizure-onset patterns in neocortical epilepsy. Epilepsia 41:297–307.

Li H, Weiss SR, Chuang DM, Post RM, Rogawski MA (1998): Bidirectional synaptic plasticity in the rat basolateral amygdala: Characterization of an activity-dependent switch sensitive to the presynaptic metabotropic glutamate receptor antagonist 2S-α-ethylglutamic acid. J Neurosci 18:1662–1670.

Luat AF, Asano E, Juhasz C, Chandana SR, Shah A, Sood S, Chugani HT (2005): Relationship between brain glucose metabolism positron emission tomography (PET) and electroencephalography (EEG) in children with continuous spike-and-wave activity during slow-wave sleep. J Child Neurol 20:682–690.

Lucignani G, Tassi L, Fazio F, Galli L, Grana C, Del Sole A, Hoffman D, Francione S, Minicucci F, Kahane P, Messa C, Munari C (1996): Double-blind stereo-EEG and FDG PET study in severe partial epilepsies: Are the electric and metabolic findings related? Eur J Nucl Med 23:1498–1507.

Machado-Salas JP (1984): Abnormal dendritic patterns and aberrant spine development in Bourneville's disease—A Golgi survey. Clin Neuropathol 3:52–58.

Malenka RC (1994): Synaptic plasticity in the hippocampus: LTP and LTD. Cell 78:535–538.

Muzik O, Chugani DC, Shen C, da Silva EA, Shah J, Shah A, Canady A, Watson C, Chugani HT (1998): Objective method for localization of cortical asymmetries using positron emission tomography to aid surgical resection of epileptic foci. Comput Aided Surg 3:74–82.

Nekhorocheff MI (1950): Use of sleep for EEG evaluation in convulsive children. Rev Neurol 83:570–575.

Olson DM, Chugani HT, Shewmon DA, Phelps ME, Peacock WJ (1990): Electrocorticographic confirmation of focal positron emission tomographic abnormalities in children with intractable epilepsy. Epilepsia 31:731–739.

Panet-Raymond D, Gotman J (1990): Can slow waves in the electrocorticogram (ECoG) help localize epileptic foci? Electroencephalogr Clin Neurophysiol 75:464–473.

Pascual-Leone A, Valls-Sole J, Wassermann EM, Hallett M (1994): Responses to rapid-rate transcranial magnetic stimulation of the human motor cortex. Brain 117:847–858.

Phelps ME, Mazziotta JC (1985): Positron emission tomography: Human brain function and biochemistry. Science 228:799–809.

Pfund Z, Chugani DC, Juhasz C, Muzik O, Chugani HT, Wilds IB, Seraji-Bozorgzad N, Moore GJ (2000): Evidence for coupling between glucose metabolism and glutamate cycling using FDG PET and 1H magnetic resonance spectroscopy in patients with epilepsy. J Cereb Blood Flow Metab 20:871–878.

Pietrzyk U, Herholz K, Fink G, Jacobs A, Mielke R, Slansky I, Würker M, Heiss WD (1994): An interactive technique for three-dimensional image registration: Validation for PET, SPECT, MRI and CT brain studies. J Nucl Med 35:2011–2018.

Rintahaka PJ, Chugani HT (1997): Clinical role of positron emission tomography in children with tuberous sclerosis complex. J Child Neurol 12:42–52.

Roach ES, Gomez MR, Northrup H (1998): Tuberous sclerosis complex consensus conference: Revised clinical diagnostic criteria. J Child Neurol 13:624–628.

Shah AK, Fuerst D, Sood S, Asano E, Ahn-Ewing J, Pawlak C, Chugani HT (2007): Seizures lead to elevation of intracranial pressure in children undergoing invasive EEG monitoring. Epilepsia 48:1097–1103.

Spanaki MV, Siegel H, Kopylev L, Fazilat S, Dean A, Liow K, Ben-Menachem E, Gaillard WD, Theodore WH (1999): The effect of vigabatrin (γ-vinyl GABA) on cerebral blood flow and metabolism. Neurology 53:1518–1522.

Szelies B, Herholz K, Heiss WD, Rackl A, Pawlik G, Wagner R, Ilsen HW, Wienhard K (1983): Hypometabolic cortical lesions in tuberous sclerosis with epilepsy: Demonstration by positron emission tomography. J Comput Assist Tomogr 7:946–953.

Szelies B, Mielke R, Kessler J, Heiss WD (1999): EEG power changes are related to regional cerebral glucose metabolism in vascular dementia. Clin Neurophysiol 110:615–620.

Theodore WH (1988): Antiepileptic drugs and cerebral glucose metabolism. Epilepsia 29 (Suppl 2):S48–S55.

Valladares-Neto DC, Buchsbaum MS, Evans WJ, Nguyen D, Nguyen P, Siegel BV, Stanley J, Starr A, Guich S, Rice D (1995): EEG delta, positron emission tomography, and memory deficit in Alzheimer's disease. Neuropsychobiology 31:173–181.

von Stockhausen HM, Theil A, Herholz K, Pietrzyk U (1997): A convenient method for topographical localization of intracranial electrodes with MRI and a conventional radiograph. Neuroimage 5:S514 (abstract).

Wilson CL, Khan SU, Engel J Jr, Isokawa M, Babb TL, Behnke EJ (1998): Paired pulse suppression and facilitation in human epileptogenic hippocampal formation. Epilepsy Res 31:211–230.